Izquierdo Barrientos, M., Sobrino, C. Almendros Ibáñez, J.A., Barreneche, C., Ellis, N. y Cabeza, L. F. (2016). Characterization of granular phase change materials for thermal energy storage applications in fluidized beds. *Applied Energy*, 181, pp. 310-321

DOI: https://doi.org/10.1016/j.apenergy.2016.08.081

Characterization of granular phase change materials for thermal energy storage applications in fluidized beds

M.A. Izquierdo-Barrientos [a], C. Sobrino [a], J.A. Almendros-Ibáñez [b,c,*], C. Barreneche [d], N. Ellis [e], L.F. Cabeza [d]

[a] Universidad Carlos III de Madrid, ISE Research Group, Thermal and Fluid Engineering Department, Avda. de la Universidad 30, 28911 Leganés, Madrid, Spain
[b] Escuela de Ingenieros Industriales, Dpto. de Mecánica Aplicada e Ingeniería de Proyectos, Castilla-La Mancha University, Campus universitario s/n, 02071 Albacete, Spain
[c] Renewable Energy Research Institute, Section of Solar and Energy Efficiency, C/ de la Investigación s/n, 02071 Albacete, Spain
[d] GREA Innovació Concurrent, Universitat de Lleida Edifici CREA, Pere de Cabrera s/n, 25001 Lleida, Spain
[e] Department of Chemical and Biological Engineering, University of British Columbia, Vancouver V6T 1Z3, Canada

abstract

This work investigates commercially available granular phase change materials (PCMs) with different transition temperatures for the use of thermal-energy storage systems in fluidized beds. The hydrody-namic characteristics of granular PCMs were tested in cylindrical-3D and planar-2D fluidized beds. The density, particle size distribution and angle of repose were measured for various PCM materials. Further attrition studies were conducted with changes in particle surface from abrasion, which were characterized using a Scanning Electron Microscope (SEM). The results indicate that some materials with smaller particle size and thinner supporting structure can lose the paraffin during the fluidization pro-cess, when paraffin is in a liquid state. As a consequence, the particles agglomerate, and the bed deflu-idizes. For all of the tested materials, only GR50 (with a transition temperature of 50 °C) properly fluidizes when the paraffin is in the liquid state and has shown to endure >75 h of continuous operation and 15 melting-solidification cycles in a fluidized bed. Additional differential scanning calorimetry (DSC) measurements of the cycled particles did not show a decrease in energy storage capacity of the granular PCM, which corroborates that there is no loss of material after >75 h of fluidization.

Keywords:
PCM
Thermal energy storage
Fluidized beds
Angle of repose
DSC

highlights

- Granular PCMs are tested in 3D and 2D fluidized beds.
- Density, particle size and angle of repose were measured for different granular PCMs.
- DSC measurements confirm that there is no loss of material after fluidization.

1. Introduction

To satisfy the global energy demand, thermal energy storage (TES) is a promising technique to complement the variability in renewable energy supplies and increase the market demand [1]. In this context, phase change materials (PCMs), which use latent heat storage, are an attractive alternative to sensible heat materials in either shell-and-tube storage systems [2] or dual-media (solid particles-fluid) energy storage tanks because they provide high storage density [3]. In this case, the PCM is encased in capsules of different geometries and sizes. The advantage of the encapsula-tion is its applicability for both liquid and air as heat transfer fluids because they are easily handled and maintain their macroscopic solid state during the solid-liquid transition. Encapsulated PCMs in small particles (micro-encapsulation) have high heat transfer area between the particles and the heat transfer fluid.

In the literature, there are studies of packed beds of macro-encapsulated spheres of PCM with diameters of a few centimeters and water as the heat transfer fluid [4,5]. In addition to these bound PCMs, granular phase-changing composites with small par-ticle diameters (1–3 mm) have been tested in latent heat thermal-storage packed beds [6,7] using air as the heat transfer fluid and in combination with a compressed-air energy storage system [8].

* Corresponding author at: Escuela de Ingenieros Industriales, Dpto. de Mecánica Aplicada e Ingeniería de Proyectos, Castilla-La Mancha University, Campus universitario s/n, 02071 Albacete, Spain.

E-mail address: jose.almendros@uclm.es (J.A. Almendros-Ibáñez).

Nomenclature

AOR	angle of repose [°]
d_p	mean particle size [mm]
DSC	Differential Scanning Calorimetry
EDS	Energy Dispersive Spectroscopy
PCM	Phase Change Material
PSD	Particle Size Distribution
SEM	Scanning Electron Microscope
T	temperature [°C]
T_{pcm}	transition temperature of the granular PCM [°C]
T_{peak}	peak temperature [°C]
U	superficial gas velocity [m/s]
$\dot{V}$	volumetric flow rate [l/min]
z	axial coordinate in the bed [cm]

Greek symbols

ΔH	enthalpy change [J/kg]
ρ	density [kg/m^3]
σ	standard deviation

Subscripts

fus	fusion
in	inlet conditions
mf	at minimum fluidization conditions
sol	solidification

Pitié et al. [9] also studied the potential use of granular PCMs in a high-temperature (500–750 ° C) circulating fluidized bed. They concluded that the PCM would help to reduce the temperature in the tubes and circulation rate of the particles, although granular materials for such high temperatures remain to be developed and manufactured.

Previously, we have published different works on granular phase change materials for low-temperature storage applications in bubbling fluidized beds [7,10–12], as an alternative to the traditional packed beds. The authors have observed that a fluidized bed of granular PCM has higher charging efficiencies during the charging process than a fluidized bed of sand or a packed bed of the identical granular material. The heat transfer coefficient between the particles and a heated surface, which is immersed in the bed, is also notably augmented in a fluidized bed with granular PCM because of the latent heat of the particles, when the bed works at approximately the transition temperature of the PCM. In all previous works, the authors used the same commercial product available from Rubitherm: "*GR bound PCM*", which consists of an inorganic matrix in which the PCM is adsorbed and rigidly bounded irrespective of whether the PCM is solid or liquid form. Different paraffins can be used as PCM in the granular material, depending on the transition temperature desired. In our case, we used the material GR50 with a transition temperature of approximately 50 °C. This material was properly fluidized at temperatures below and above this transition temperature and did not present agglomeration problems. Although it suffered some attrition after 75 h of continuous operation with 15 charging-discharging cycles, no evidence of loss of PCM was observed.

In the present work, we tested the same commercial product, "*GR bound PCM*" from Rubitherm, but commercialized with different phase change temperatures: GR42 and GR80, with transition temperatures of approximately 42 °C and 80 °C, respectively. The first experimental observations showed that GR42 and GR80 did not properly fluidized at temperatures above the transition temperature: the particles agglomerated, and the bed was defluidized.

To understand the agglomeration behavior of various granular phase-changing composites, where two of three materials have

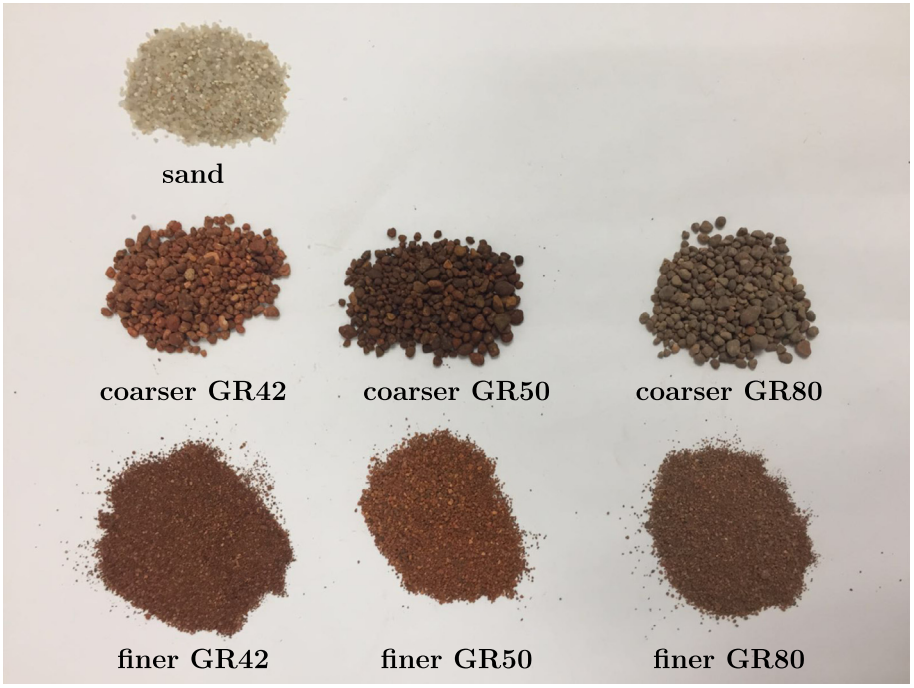

Fig. 1. Images of different granular PCMs that are used for sensible heat storage, and silica sand is also shown as a reference.

Table 1
Density [kg/m^3] of the different granular PCM tested in this work. The density of the sand used by Izquierdo-Barrientos et al. [7] is also indicated.

	Sand $\rho = 2632.3 \pm 1.2$ Granular PCM	
	Finer PCM	Coarser PCM
GR42	$\rho = 1531.7 \pm 0.7$	$\rho = 1563.1 \pm 0.4$
GR50	$\rho = 1550.5 \pm 1.0$	$\rho = 1512.8 \pm 1.6$
GR80	$\rho = 1594.7 \pm 1.6$	$\rho = 1618.0 \pm 0.3$

agglomeration problems when they are heated in a fluidized bed, the hydrodynamic characteristics of the materials in fluidized beds are studied in this paper. The angle-of-repose measurements, attrition testing and SEM observations are used to understand the different behaviors of these materials. The DSC measurements are finally performed to check the differences in thermal behavior of the suitable material to fluidize after several heating cycles.

2. Materials

The commercial product employed in this work is "*GR bound PCM*", which is commercialized by Rubitherm [13] and suitable for low-temperature energy storage applications (−10 °C to 90 °C). Three different materials with three different phase change temperatures were tested: GR42, GR50 and GR80. The number corresponds to their approximate phase change temperature T_{pcm}. Fig. 1 shows a picture of different PCMs and a picture of the silica sand in the experiments of Izquierdo-Barrientos et al. [7], which is a common sensible storage material and was used as a reference material. The external appearance of the granular PCMs is similar to any other granular material, regardless of whether the PCM is in the liquid or solid state. The granular PCM is composed of paraffin (∼30 wt.%), which is the phase-changing component, and a natural porous material. The paraffin is different in each material to get the desired transition temperature. The inorganic component behaves similarly to a sponge, where the organic PCM is adsorbed during the manufacturing process. The PCM is rigidly bound to the inorganic matrix regardless of whether the PCM is in the solid or liquid state. The granular material has been developed to be easily handled. These granular PCMs are available in two sizes with particle diameters of 1–3 mm (coarser size) and 0.2–0.6 mm (finer size). These materials were used by different researchers for thermal-energy storage applications in fixed [6,7] and fluidized beds Izquierdo-Barrientos et al. [7,10].

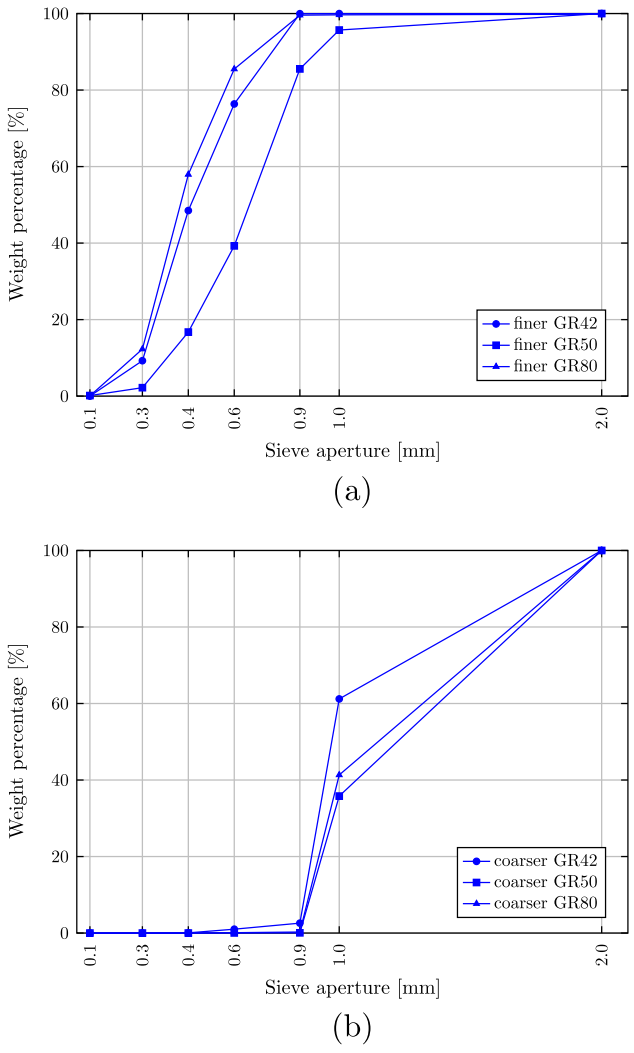

Fig. 2. Particle size distribution of the finer and coarser granular PCMs: GR42, GR50 and GR80.

2.1. Density, size distribution and minimum fluidization velocity

The two main properties of any granular material to be fluidized are their density and size, which can be categorized according to Geldart [14] to predict the fluidization behavior of these materials. The particle density of the granular PCMs has been determined using a helium pycnometer AccuPyc 1340 of micromeritics. This device uses the gas displacement method to measure the volume occupied by the sample, and the density is calculated as the ratio of the mass to its volume; the mass is invariably measured on a discrete device. Table 1 shows the density of different granular PCMs. There is no noticeable difference among the different gran-ular PCMs. The density of the granular PCMs is notably lower than other typical materials in fluidized beds. Izquierdo-Barrientos et al.[7,10] experimentally and numerically compared the thermal behavior of two granular materials (finer GR50 and sand) in a

Table 2
Mean particle size [mm] of different granular PCMs in this work. The mean particle size of the sand used by Izquierdo-Barrientos et al. [7] is also indicated.

	Sand $d_p = 0.755 \pm 0.069$ Granular PCM	
	Finer PCM	Coarser PCM
GR42	$d_p = 0.368 \pm 0.066$	$d_p = 1.382 \pm 0.202$
GR50	$d_p = 0.541 \pm 0.082$	$d_p = 1.642 \pm 0.196$
GR80	$d_p = 0.334 \pm 0.069$	$d_p = 1.586 \pm 0.202$

Table 3
Minimum fluidization velocity [m/s] of different tested granular PCMs in this work. The minimum fluidization velocity of the sand used by Izquierdo-Barrientos et al. [7] is also indicated. The minimum fluidization velocity for the sand and three finer granular PCMs was experimentally measured, whereas that for the three coarser granular PCMs was calculated according to Wen and Yu [16].

	Sand $U_{mf} = 0.33$ Granular PCM	
	Finer PCM	Coarser PCM
GR42	$U_{mf} = 0.13$	$U_{mf} = 0.55$
GR50	$U_{mf} = 0.09$	$U_{mf} = 0.65$
GR80	$U_{mf} = 0.07$	$U_{mf} = 0.66$

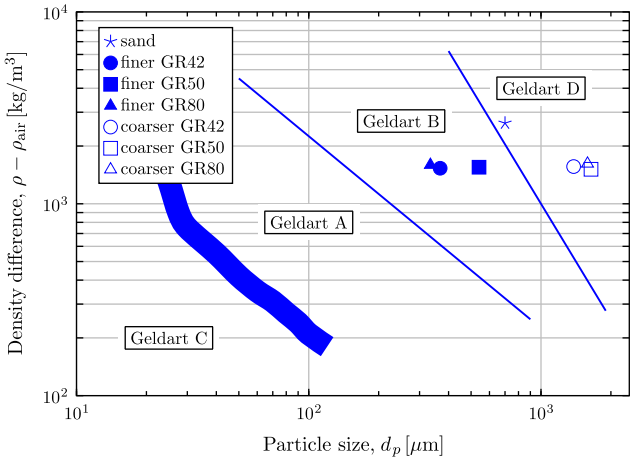

Fig. 3. Geldart diagram for particle classification [14]. The symbols indicate the location in the diagram of different granular PCMs in this work and the sand used by Izquierdo-Barrientos et al. [7].

fluidized-bed thermal-storage system. The density of the sand in these works was $\rho = 2632.3$ kg/m^3. Izquierdo-Barrientos et al. [7] observed that the lower density of GR50 enabled higher efficiencies because of the lower necessary mass flow rate to fluidize the particles.

Fig. 2(a) and (b) shows the cumulative particle size distribution, which was measured using the equipment Retsch AS-200-control with a sieve analysis for the finer and coarser granular PCMs, respectively. In these figures, the percentage in passing mass versus the sieve size is represented. Fig. 2(a) shows that the finer GR50 has a larger percentage of larger particles than the other two finer materials, whereas the coarser GR42 has a larger percentage of particles with a size under 1 mm (see Fig. 2(b)). Table 2 indicates the mean particle size of each material, which was calculated with the particle size distribution, and its standard deviation. For comparison purposes, the mean particle size of the sand that Izquierdo-Barrientos et al. [7] used in their experiments is also indicated. The larger mean particle size of the finer GR50, compared to GR42 and GR80, indicates a thicker boundary structure of this material in comparison with the other two.

The minimum fluidization velocity U_{mf} of the three thinner materials was determined by measuring the pressure drop across the bed as a function of the superficial gas velocity. The minimum fluidization velocity is commonly defined as the intersection of the horizontal fluidized bed line and the sloping packed bed line [15]. Table 3 shows U_{mf} of the finer PCMs materials. U_{mf} of the coarser PCMs was not experimentally measured because they are higher than the maximum superficial gas velocity that our facility can supply. These velocities were estimated according to Wen and Yu [16].

Fig. 3 shows the original Geldart diagram [14] where different particle types are indicated. In this diagram, the finer granular PCMs in this work are indicated with solid points, which are clearly particles type B. This type of particles fluidizes with a vigorous bubbling behavior and presents a good circulation and mixing of solids. The coarser granular PCMs are indicated with empty symbols. These particles belong to type D particles, which do not easily fluidize, and large amounts of gas are required. This type of particles can be used in spouted beds and/or fixed and moving beds,

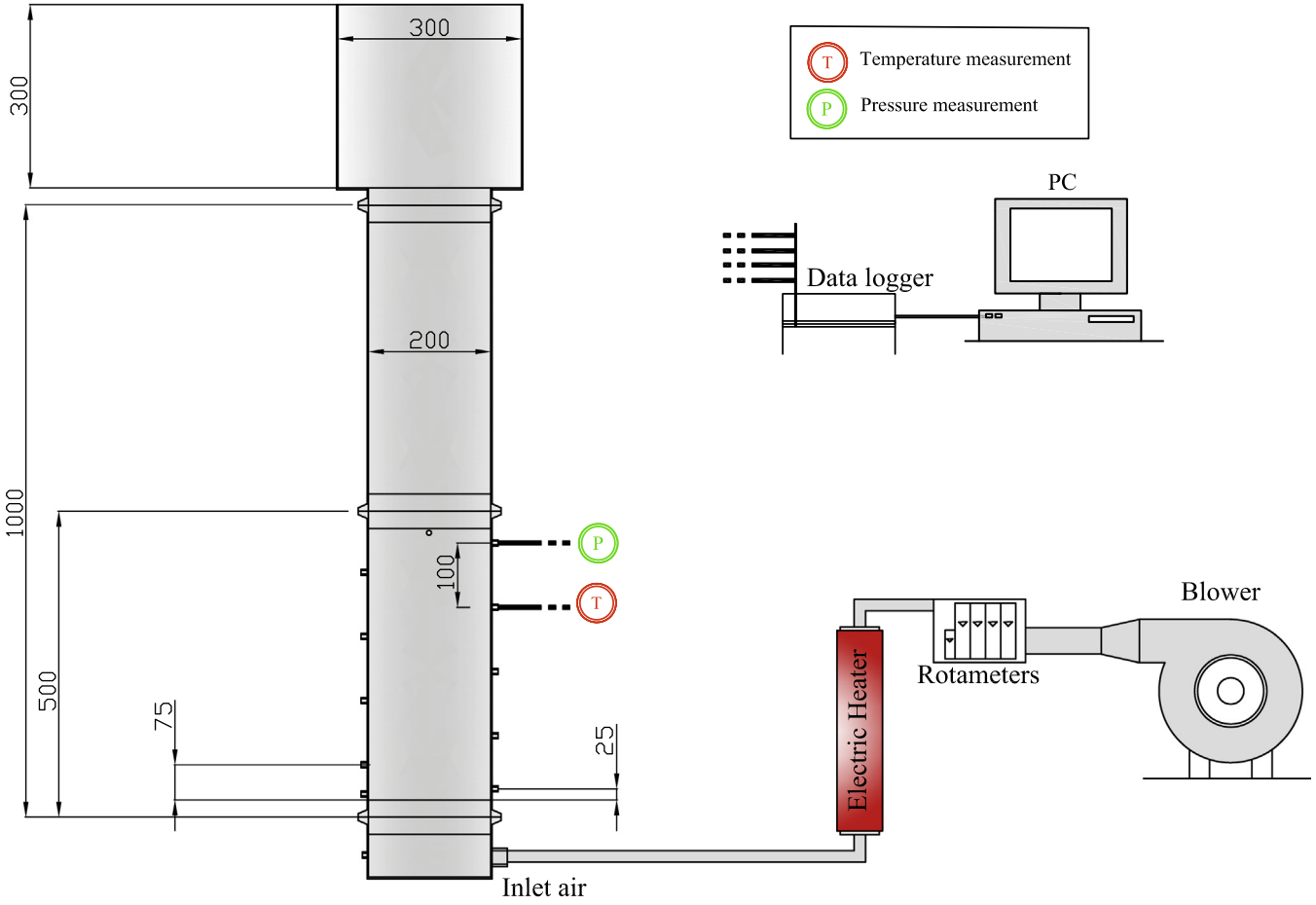

Fig. 4. Schematic representation of the 3D-cylindrical fluidized bed. Dimensions in mm.

which is beyond the scope of this work. In this figure, the sand used by Izquierdo-Barrientos et al. [7] is indicated with a star. Although this point is in group D particles, it is notably close to Geldart B. Izquierdo-Barrientos et al. [7] experimentally observed a particle behavior similar to that of type B with a bubbling behavior.

Considering Fig. 3, the finer granular PCMs appear appropriate to use in a bubbling fluidized bed and will be the selected material in the fluidization experiments in this paper. Although GR42 and GR80 have smaller particle size than GR50, they belong to group B particles and are far from the limit of group C particles (cohesive particles), where the interparticle forces are strong and hinder the fluidization process. Thus it is speculated that the interparticle forces are not the dominate force in causing the observed agglomeration in the finer materials GR42 and GR80. The required air flow rate to fluidize the coarser granular PCM would be too high, which discard their use in a bubbling fluidized bed. In the following section, we describe the behavior of the finer GR42 and GR80 in two experimental set-ups: cylindrical-3D and planar-2D fluidized beds. The 2D bed enables us to observe the interior of the bed.

3. Fluidization experiments

3.1. Experimental set-ups

The finer granular PCMs were fluidized in two experimental set-ups. First, the materials were tested in a cylindrical-3D fluidized bed (identical to that used by Izquierdo-Barrientos et al. [7,10]). Second, to visually corroborate the results in the 3D facility, a planar-2D fluidized bed was used, which enables a visual inspection of the fluidization process.

The cylindrical-3D fluidized bed is illustrated in Fig. 4. The bed consisted of a cylindrical tube of ID 200 mm stainless steel with 2 mm thick walls. A fine mesh screen was mounted at the bottom of the distributor plate to prevent the solid particles from entering the plenum chamber. The air entered the plenum of the column and flowed into the bed through a distribution plate with a thickness of 1.5 mm, which contained 300 perforations with a diameter of 2 mm, which resulted in a 3% open area. The instrumentally monitored section of the test apparatus was 500 mm high and insulated with 20-mm-thick glass wool. Additionally, the column was insulated with a 10-mm-thick thermal insulator. The expanded freeboard had an internal diameter of 300 mm. The air flow was supplied by a blower with a variable mass flow rate and heated by electrical heaters, which were regulated by a PID controller before flowing into the column. Type K thermocouples were used to measure the temperature at specific locations in the test section and plenum chamber. At these locations, the pressure variations could be measured using pressure sensors with two different ranges: 100 mbar and 1 bar.

Fig. 5 shows a scheme of the planar-2D fluidized bed, which is identical to that used by [17]. The experimental apparatus is a two-dimensional fluidized column with inner dimensions of 310 × 16 × 510 mm, which was designed to operate at a maximum pressure of 2170 kPa. The fluidized bed was constructed of 43 mm

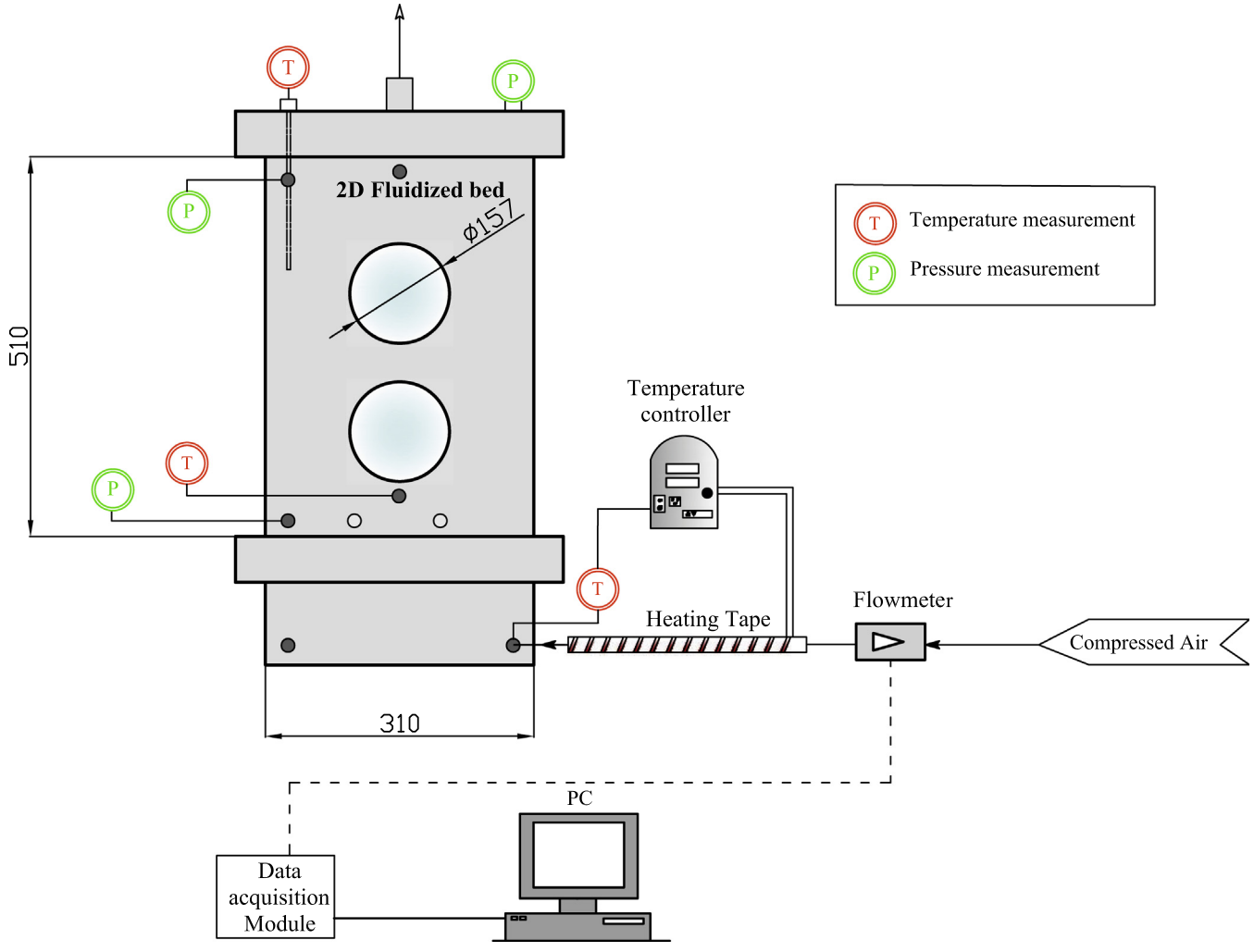

Fig. 5. Schematic representation of the planar-2D fluidized bed. Dimensions in mm.

thick steel plates. To view the fluidization phenomena, four tempered glass windows of 157-mm diameter and 25.4-mm thickness were used. The windows were placed in pairs on opposite faces of the column and maintained in place using silicon. Then, a gasket was placed outwards over the windows and steel plates to prevent the windows from sliding outwards. A metal mesh was used as the distributor, and additional mesh were used to prevent the backflow of particles, which would clog the bed fittings. The gas supply for the fluidized bed derived from the compressed air from the building air line and was preheated before entering the column by a heating tape. To control the inflow of gas into the fluidized bed, the flow rate was controlled by regulators and more precisely with needle valves.

3.2. Experimental results

Fig. 6 shows the temperature profile obtained by Izquierdo-Barrientos et al. [7] in the cylindrical-3D bed with finer GR50, which was fluidized at U/U_{mf} of 1.5, 2.0 and 2.5. The bed was filled with 5 kg of GR50, which resulted in a bed height at minimum fluidization conditions of approximately $H_{mf} \approx D = 20$ cm. Four thermocouples measured the temperature at 2.5 cm, 7.5 cm, 12.5 cm and 17.5 cm above the distributor. Two additional thermocouples measured the air temperature at the bed inlet, below the distributor, and at the exit. Three experiments were performed with three different flow rates: 375, 500 and 625 l/min, which corresponded with superficial gas velocities of 0.2, 0.27 and 0.33 m/s, respectively. Hence, according to the minimum fluidization velocity of the material GR50 (see Table 3), the experiments were performed at an excess gas velocity over minimum fluidization conditions of $U/U_{mf} = 1.5$, 2.0 and 2.5. In all cases, the air was heated to a tem-perature of 65 °C, and the particles in the bed were heated for 2–3 h. Then, the electrical resistance that heated the air was switched off, the air and particles were cooled, and the temperature was measured.

Three thermocouples at 7.5 cm, 12.5 cm and 17.5 cm above the distributor measured the identical temperature, which indicates the well-mixed state in the bubbling fluidized bed. Only the thermocouple near the distributor (2.5 cm above it) showed a higher temperature. This thermocouple could be affected by the air jets from the distributor and measured a temperature closer to the temperature of the inlet air [18].

Fig. 7 shows the experimental results with the granular PCMs GR42 and GR80, which were tested under the identical experimental conditions of Izquierdo-Barrientos et al. [7] with GR50, as shown in Fig. 6. These materials have a smaller mean particle size than GR50 and consequently lower U_{mf}. Because the experiments with materials GR42 and GR80 were performed with constant superficial gas velocities of $U = 0.20$, 0.27 and 0.33 m/s, the excess velocities over minimum fluidization velocity with identical gas flow rates are higher for the experiments with these materials. Contrary to the experimental results of the finer GR50 [7], these materials did not properly fluidize when the temperature of the bed was higher than the transition temperature of each material

(T_{pcm}). For example, in Fig. 7(b) (GR80 with $\dot{V} = 375$ l/min), the bed behaved as a well-mixed tank up to nearly 80 °C; however, beyond this temperature, the bed temperature progressively increased from the bottom to the top of the bed as in a plug-flow system. This behavior is typical of fixed beds and indicates that the bed was defluidized. This anomalous behavior appeared to be mitigated when the gas flow rate increased. For GR80 with a gas

flow rate of $\dot{V} = 625$ l/min, which corresponds with an excess gas velocity of $U/U_{mf} = 4.4$, the bed was well mixed. Similar experimental results were obtained for GR42.

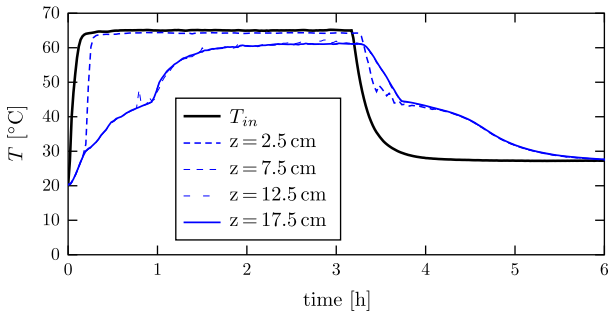

(a) $\dot{V} = 375\,\mathrm{l/min}$, $U/U_{mf} = 1.5$

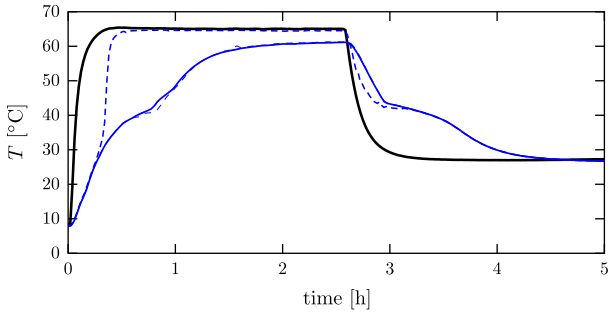

(b) $\dot{V} = 500\,\mathrm{l/min}$, $U/U_{mf} = 2.0$

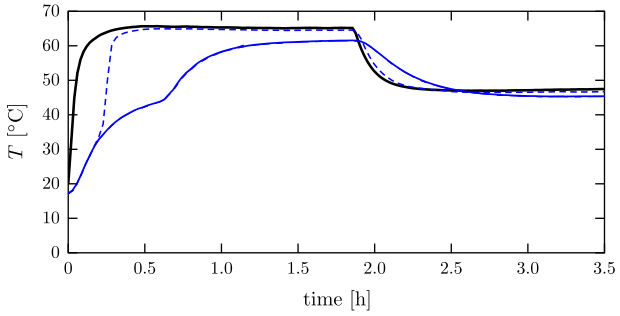

(c) $\dot{V} = 625\,\mathrm{l/min}$, $U/U_{mf} = 2.5$

Fig. 6. Temperature variations in the cylindrical-3D bed with the finer GR50. The legend of Figures (b) and (c) is identical to that of Figure (a).

The differences in the hydrodynamic behavior of GR50, GR42 and GR80 are related with the different particle sizes and the characteristics of the natural porous material used as a matrix where the PCM material was bound. Because this supporting material might not be homogenous in composition, it could have different performances to avoid the leakage of the paraffin. In the case of GR42 and GR80, some paraffin leaked from the supportive structure; when paraffin melted during the charging process, it served as an adhesive, which made the granules stuck together and caused the bed to defluidize. Furthermore, when the bed was cooled below the phase change temperature, the paraffin solidified, and the fluidizing air broke the agglomerates and re-fluidized the bed. This re-fluidization only occurred for experiments where the air flow rate was sufficiently large to produce a vigorous bubbling of the bed.

Additional experiments were performed in the planar-2D facility to observe the fluidization quality and bed behavior. Fig. 8 shows three pictures where the bed interior is observed through one of the windows of the bed. Fig. 8(a) shows the fluidization process of GR42 when the bed temperature was below the transition

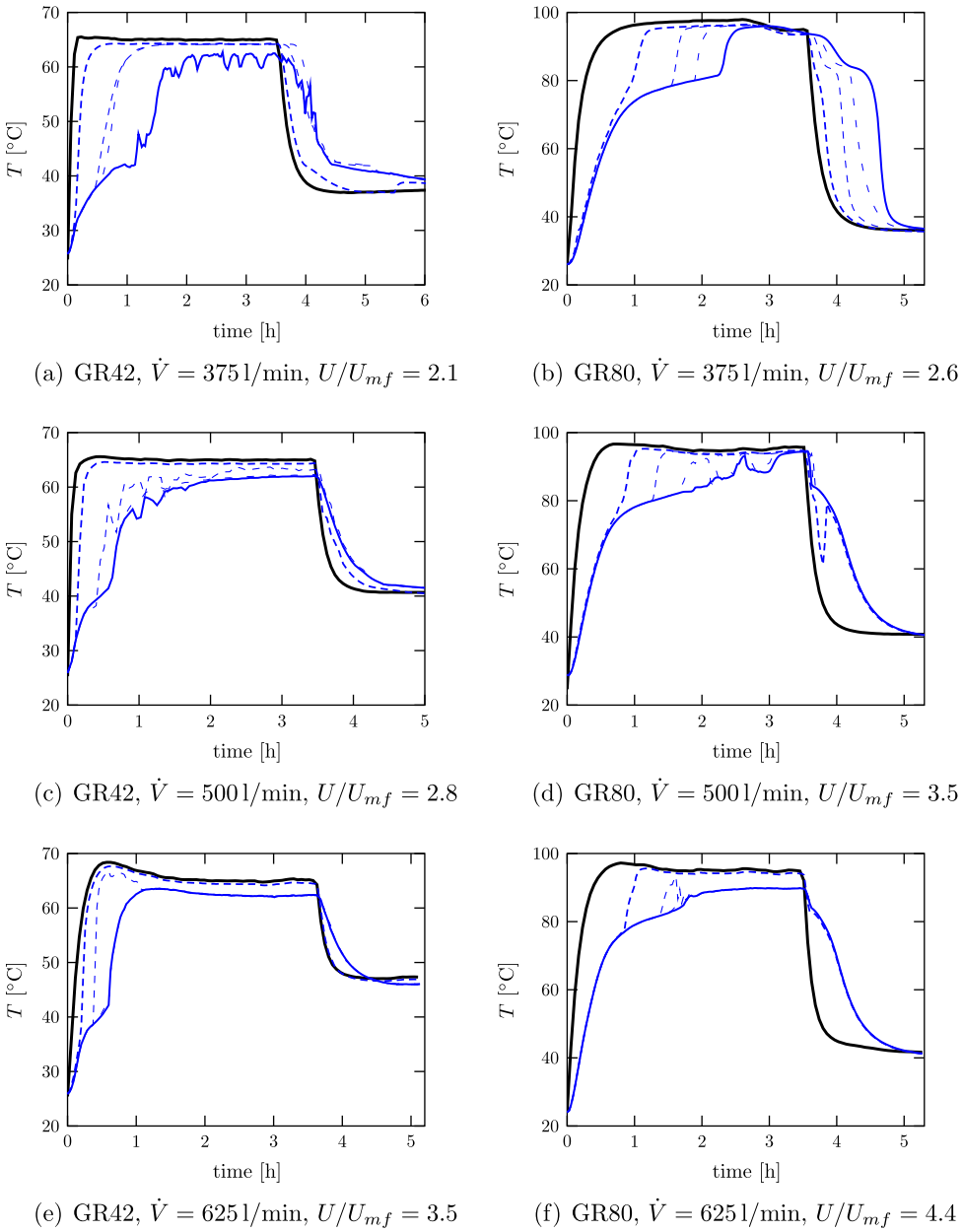

(a) GR42, $\dot{V} = 375\,\mathrm{l/min}$, $U/U_{mf} = 2.1$

(b) GR80, $\dot{V} = 375\,\mathrm{l/min}$, $U/U_{mf} = 2.6$

(c) GR42, $\dot{V} = 500\,\mathrm{l/min}$, $U/U_{mf} = 2.8$

(d) GR80, $\dot{V} = 500\,\mathrm{l/min}$, $U/U_{mf} = 3.5$

(e) GR42, $\dot{V} = 625\,\mathrm{l/min}$, $U/U_{mf} = 3.5$

(f) GR80, $\dot{V} = 625\,\mathrm{l/min}$, $U/U_{mf} = 4.4$

Fig. 7. Temperature variations in the cylindrical-3D bed with the finer GR42 and GR80. The legend of all figures is identical to that of Fig. 6(a).

temperature of the material with a gas flow rate slightly higher than the minimum fluidization conditions. Small ascending bubbles were observed in the bed, which indicates that the bed was properly fluidized. In contrast, when the bed temperature was increased beyond T_{pcm}, the bubbles disappeared, and the particles appeared to become agglomerated, as observed in Fig. 8(b). The increase in gas flow rate in an attempt to re-fluidize the bed was not successful in the 2D geometry. Instead, small channels were observed among the agglomerated particles (see Fig. 8(c), which enabled the gas to by-pass the bed.

From the fluidization experiments, it is concluded that the materials GR42 and GR80 do not properly fluidize when the temperature of the bed is higher than their transition temperatures, i.e., 42 °C and 80 °C, respectively. When the granular PCM is above its transition temperature, the paraffin is in the liquid state and can leak out of the granule and act as a binder. Consequently, the particles tend to agglomerate, and the bed defluidizes.

4. Analysis of the granular PCMs

This section describes the results of additional experimental measurements to explain the observed differences in the fluidization process of the materials GR42 and GR80 when the temperature is above their transition temperature.

4.1. Angle of repose

The angle of repose is generally accepted as an indirect measurement of the characteristics of a bulk of particles to flow, i.e., its flowability [19–21]. Geldart et al. [20] shows that the inverse of the AOR is equivalent to the cohesion measured in a standard shear tester. Krantz et al. [21] recommended dynamic testing (such as the AOR) to characterize particles to be used in applications where they are in motion (such as moving or fluidized beds),

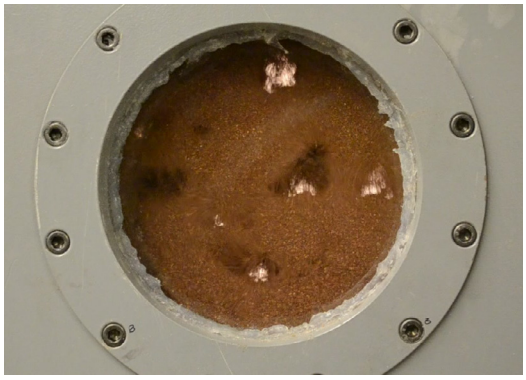

(a) good fluidization ($T < T_{pcm}$ and $U \gtrsim U_{mf}$)

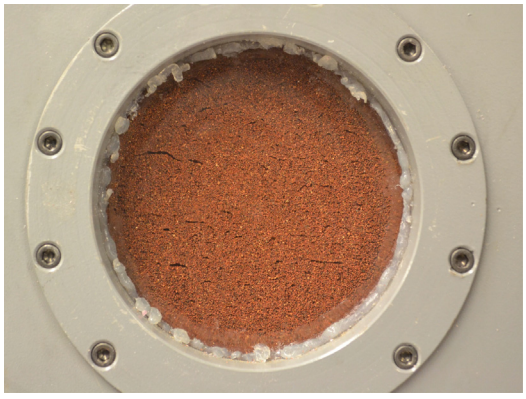

(b) agglomeration ($T > T_{pcm}$ and $U \gtrsim U_{mf}$)

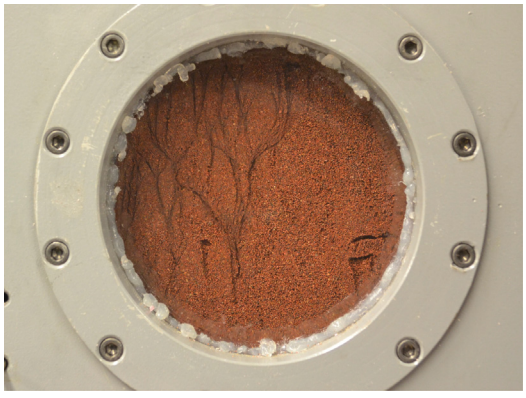

(c) channeling ($T > T_{pcm}$ and $U \gg U_{mf}$)

Fig. 8. Visual observation of the fluidization process of the finer GR42.

whereas static testing (such as shear cell methods) appears more appropriate to characterize powders to be used in packed beds. The angle of repose is commonly defined as the angle formed by a bulk of particles when they are poured through a funnel and forms a conical pile. The angle formed by the base of the cone and its generatrix is the angle of repose. Various authors [22,19] have proposed a limiting value of $AOR = 40°$. The bulk of particles above this value do not properly flow.

The angle of repose was measured for the three finer granular materials GR42, GR50 and GR80 in the identical device to that developed by Geldart et al. [19]. Fig. 9 shows the angle of repose, which was obtained as the average value of seven runs, for the three materials at room temperature. Approximately 25 s were required to pour the entire sample. No noticeable differences

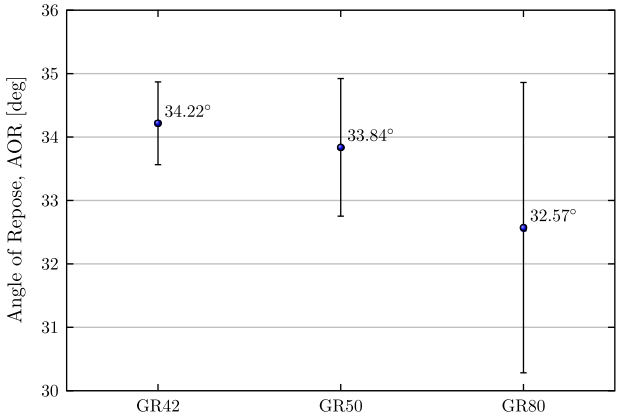

Fig. 9. Angle of repose of the three finer granular PCMs at room temperature.

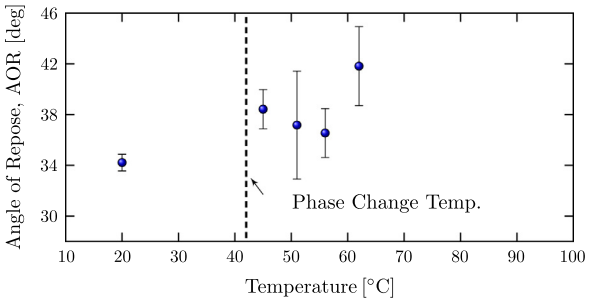

(a) GR42

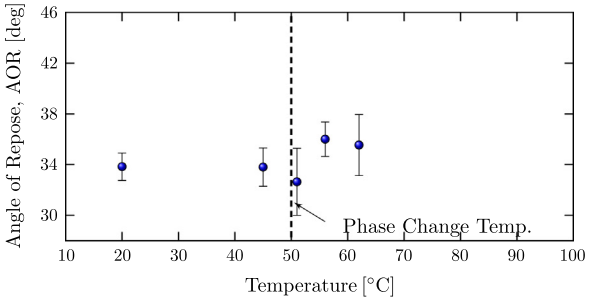

(b) GR50

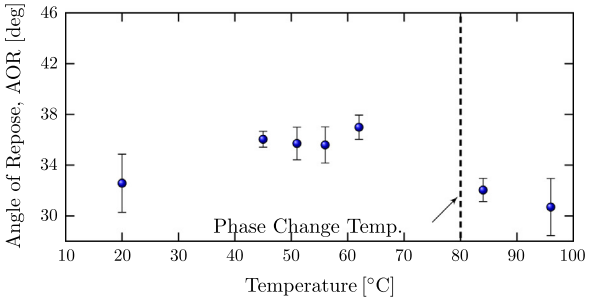

(c) GR80

Fig. 10. Variation of the angle of repose with temperature for the three materials.

appeared among the three materials. Because of the large error bars, it is not possible to delineate a clear trend with the angle of repose. Nevertheless, Chauvenet's criterion with a 90% confidence was applied to assess whether one piece of experimental data from the set of observations was likely spurious.

Fig. 10 shows the variation of the angle of repose with temperature for the three materials to study a possible effect of the temperature on this parameter. No significant conclusions can be drawn because no remarkable changes appear in the AOR when the materials were heated beyond T_{pcm}. The angle of repose appeared unaffected by the temperature of the material. In all cases, except GR42 at a temperature above 60 °C, the angle of repose was always under 40°, which is the limit proposed by Ante-quera et al. [22] and Geldart et al. [19] for a good flowability of the material.

During the angle-of-repose measurements, some problems were observed with the materials GR42 and GR80 at temperatures above their transition temperatures. When these materials were heated beyond T_{pcm}, their flowability decreased with signs of cohesiveness. In addition, the pouring time decreased to 12 s because the materials did not flow continuously but in clumps. For example, during the AOR measurement of GR80 at a temperature of 84 ° C, the particles flowed in blocks (Fig. 11(a)), and some electro-static forces were observed in parts of the device (Fig. 11(c)). Fig. 11(b) and (d) shows different problems of agglomerations and material blocks of GR42 at 62 °C and 45 °C, respectively. These problems, which affect the fluidization behavior of different materials, are not reflected in the AOR measurement.

4.2. Attrition tests

In fluidized beds, the vigorous bubbling in the bed can provoke the attrition of the particles. If the attrition is significant, the granular PCM particles can lose part of the paraffin inside the supporting structure of SiO_2. Two different attrition mechanisms are typically observed in fluidized beds: abrasion and fragmentation [23]. In the fragmentation process, the particles are broken into smaller particles of similar sizes; in the abrasion process, fine particles are removed from the particle surface. Abrasion more frequently occurs in fluidized beds than fragmentation [24,25].

In a previous study, Izquierdo-Barrientos et al. [7] performed a cycling test to measure the particle size distribution of different samples of GR50, which were fluidized in the cylindrical 3D-facility as described in Section 3.1, during more than 75 h of con-tinuous fluidization and 15 heating-cooling cycles. The particle size

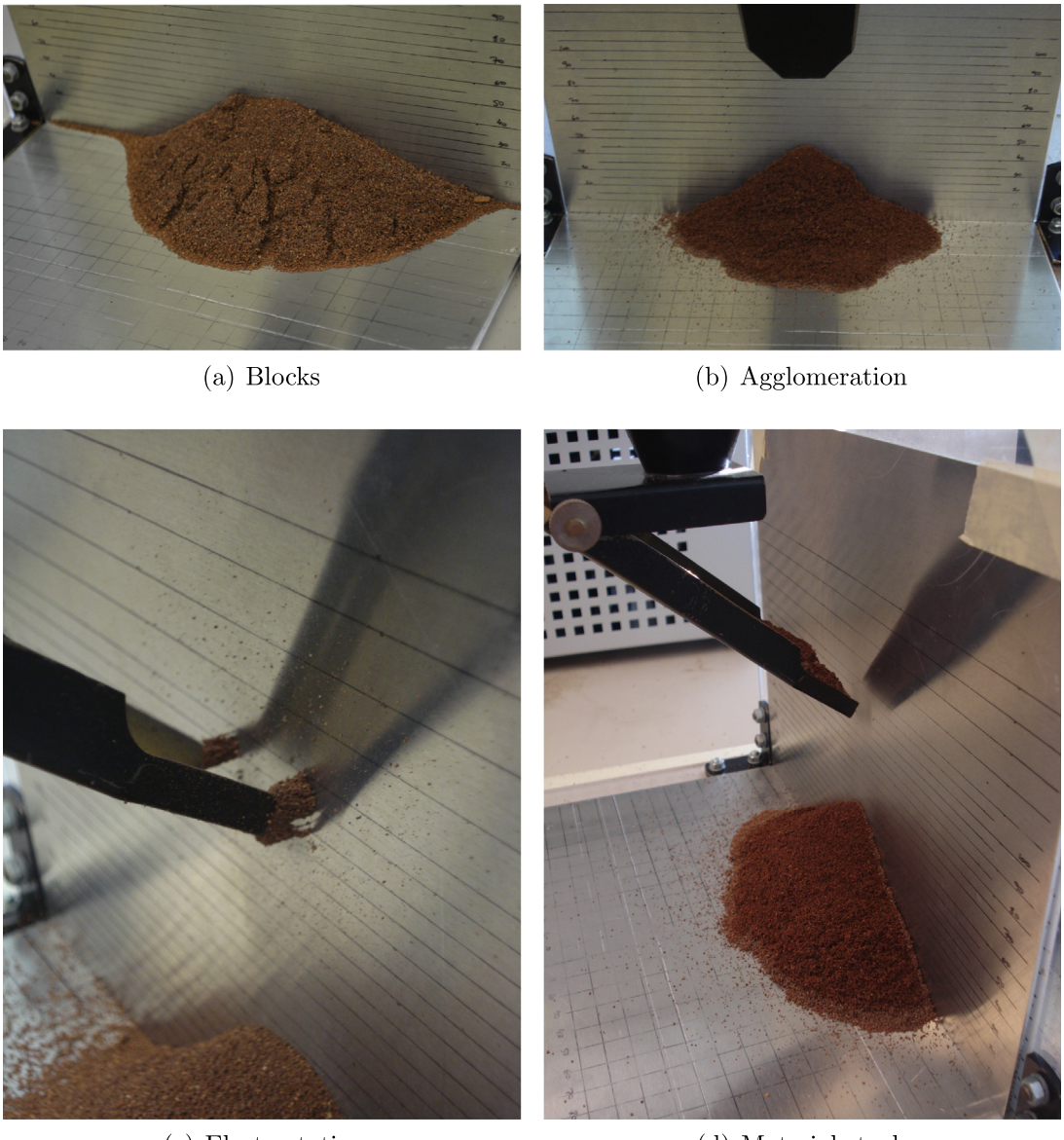

(a) Blocks (b) Agglomeration

(c) Electrostatics (d) Material stuck

Fig. 11. Different problems observed during the angle-of-repose measurement.

distribution was measured after 3, 6, 9, 12 and 15 cycles. The particle size distribution slightly decreases with the number of cycles, although fragmentation was not observed.

To characterize the attrition resistance of granular PCMs and compare the behaviors of GR42 and GR80, which exhibited agglomeration problems, with GR50, which was properly fluidized, attrition tests were performed. These tests also allowed to discard the fragmentation of particles during the fluidization process. The attrition testing apparatus follows the ASTM D5757-00 standard [26], which is a widely used standard procedure to characterize the attrition resistance of particles and powders [27,28]. It consists of four main stainless-steel components: the three-orifice (0.397 mm) distributor plate, attrition column (710 mm high, 35 mm), conically divergent/convergent freeboard settling cham-ber (630 mm high), and fine collector, which contains a ceramic fil-ter (0.1 mm pore size). The unit was loaded with 50 g of the particulate sample and operated at 10 l/min of air at room temper-ature and room pressure for 5 h.

The particle size distributions (PSDs) before and after the attrition tests for the three materials and their corresponding mean particle diameters with their standard deviations are shown in Fig. 12. The distributions are Gaussian and have similar widths. Although the mean particle diameter is slightly higher for GR50, the shape of the distribution affects the defluidization of a fluidized bed more than the mean particle size [29]. Fig. 12 shows no particle fragmentation of the materials GR42 and GR80 (a bi-modal PSD should be obtained), so fragmentation is not the cause of the loss of paraffin and agglomeration of the bed when this type of granulates is fluidized.

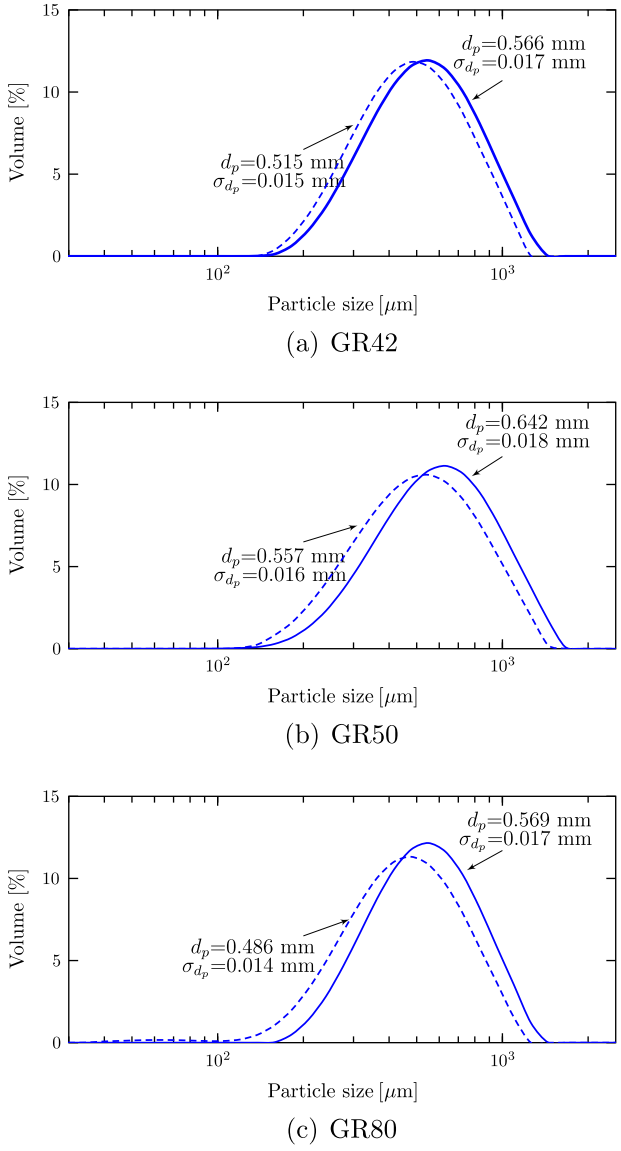

Fig. 12. Particle size distributions of (a) GR42, (b) GR50 and (c) GR80 before (continuous line) and after (dashed line) the attrition tests.

The PSDs after the attrition tests indicate that the bed particles are only slightly smaller than the original ones. Considering Fig. 12, it has been proven that attrition increases the number of particles and decreases their size (the mean diameters decreased after the attrition tests). As a consequence, the PSDs are modified, being the degree of variation of the PSD after the attrition test notably similar for the three materials. Fine particles that are smaller than 50 μm were only detected for the finer GR80 with a fraction of 0.33% of the total mass, which is not significant. Nevertheless, due to the abrasion of materials, some leakages of the PCM might occur and affect the agglomeration of the material.

4.3. Scanning Electron Microscope (SEM) observations

One more test was performed to study the structure of the granular PCMs before and after fluidization. The microstructure of the three finer PCMs was examined using a Scanning Electron Microscope (SEM) on a Jeol 6490 LV electron microscope, which was equipped with an EDS detector (Oxford INCA Energy) and detectors for secondary and backscattered electrons. Fig. 13 shows several SEM pictures for the materials GR42, GR50 and GR80 with a magnification of 2500 μm. The samples observed in the SEM were obtained before and after the fluidization experiments in the cylindrical 3D-bed in Figs. 6 and 7.

The differences in contrast are related to the changes in conductivity of the material. No significant differences were detected between the initial and post-fluidization samples. Only the topography of the post-fluidization specimens, particularly GR42 and GR80, appeared softer than the initial ones, which may indicate that part of the paraffin leaked through the secondary structure. To corroborate that some paraffin was at the surface of the particles, an Energy Dispersive Spectroscopy (EDS) analysis was performed to determine the C content at the surface. However, because of the interaction volume of the X-rays, C at the surface and C inside the particles were indistinguishable.

5. Differential Scanning Calorimetry (DSC) measurements

After the three finer granular PCMs were tested using two experimental facilities and different properties were measured, only the finer GR50 appeared appropriate for use in a fluidized bed for thermal-energy storage applications. The other two materials, GR42 and GR80, have agglomeration problems when the bed temperature is above their phase change temperature. These materials have smaller particle sizes than GR50. The external layer of porous material, which serves as a matrix to bind the PCM, may be thinner than the layer of GR50, and suffered from abrasion in the fluidization process, where some paraffin is lost and causes the particle agglomeration.

Izquierdo-Barrientos et al. [7] analyzed and compared this material with sand in a fluidized bed for thermal-energy storage. GR50 was fluidized in fifteen charging-discharging cycles between ambient temperature and 65 °C. The particles were fluidized in >75 h. After every three cycles, a sample of 250 g was extracted from the bed to measure the particle size distribution. They observed a slight decrease in mean particle size because of the abrasion.

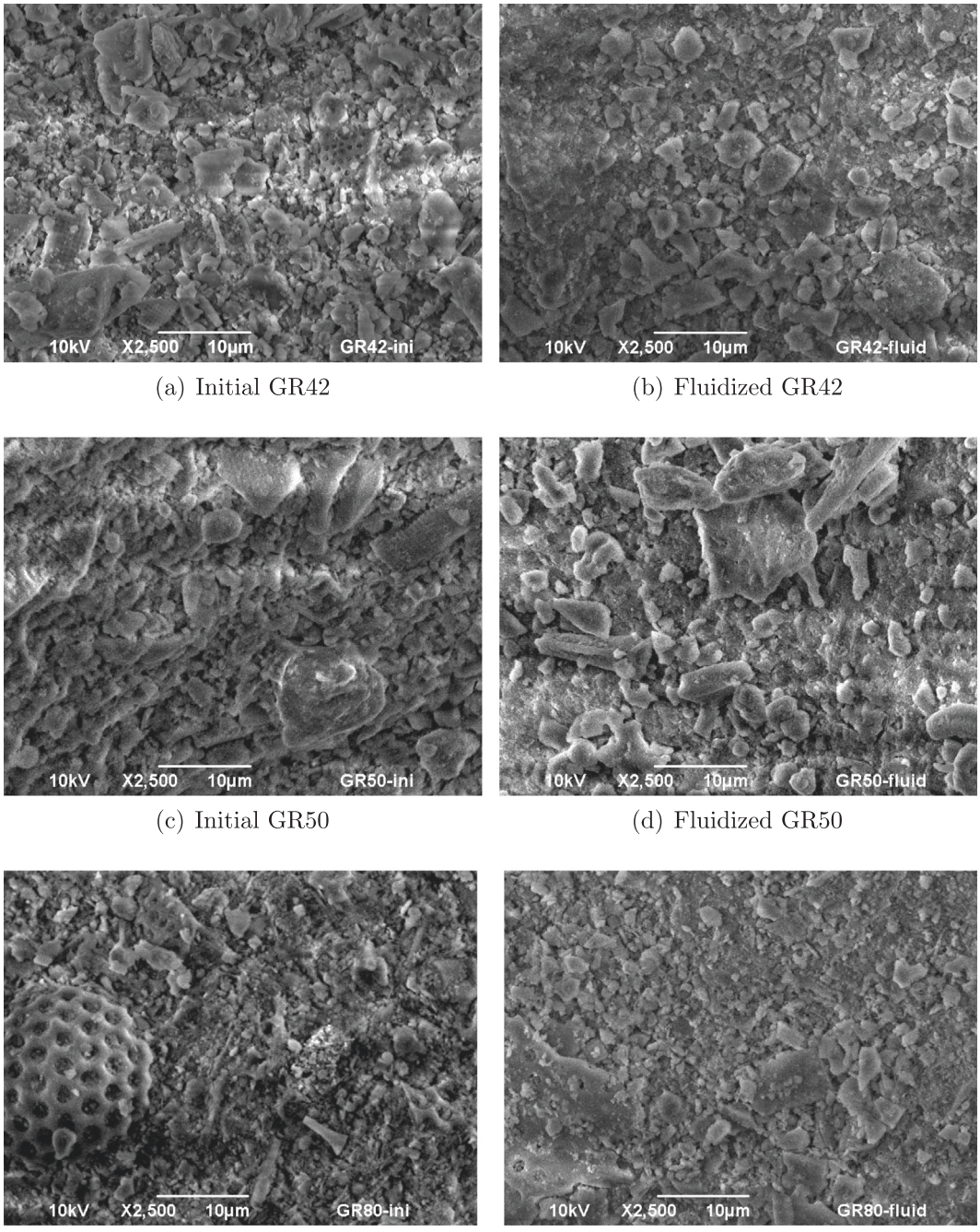

(a) Initial GR42 (b) Fluidized GR42

(c) Initial GR50 (d) Fluidized GR50

(e) Initial GR80 (f) Fluidized GR80

Fig. 13. SEM pictures before and after fluidization for the materials (a,b) GR42, (c,d) GR50 and (e,f) GR80.

Table 4
Enthalpy of fusion (ΔH_{fus}) and solidification (ΔH_{sol}) and peak temperature during the fusion ($T_{peak_{fus}}$) and solidification ($T_{peak_{sol}}$) for different samples of GR50.

	ΔH_{fus} [kJ/kg]	ΔH_{sol} [kJ/kg]	$T_{peak_{fus}}$ [°C]	$T_{peak_{sol}}$ [°C]
0 cycles	44	44	47.9	46.5
3 cycles	44	44	45.4	44.1
6 cycles	46	46	45.4	44.0
9 cycles	43	43	45.4	44.0
12 cycles	43	44	45.3	44.2
15 cycles	44	44	45.5	44.1

To corroborate that the particles of GR50 in Izquierdo-Barrientos et al. [7] did not lose the paraffin during the fluidization process, the extracted samples from the bed were analyzed in a Mettler Toledo DSC822e. A small mass of 20 mg of each sample of every three cycles was heated from 25 ℃ to 80 °C at a rate of 0.5 K/min as recommended by various authors [30,31] in previous DSC studies, which measured the PCM, maintained them at this maximum temperature for ten minutes and subsequently cooled them to the initial temperature at the same rate. The process was repeated two times with a different small mass of 20 mg of each sample.

Table 4 summarizes the main results of the DSC analysis. The table shows the enthalpy changes and peak temperatures during the fusion (ΔH_{fus}) and solidification (ΔH_{sol}) processes. There is no decrease in enthalpy with the number of cycles. The differences between the initial and cycled samples (after 3, 6, 9, 12 and 15 cycles) are smaller than the DSC error and cannot be attributed to a loss of material.

Regarding the peak temperature, there are small differences between the initial and post-fluidized materials. For the unused material, the peak temperature during the fusion process is $T_{peak_{fus}} \approx 48\ ^{\circ}C$. After three cycles, this temperature decreased but remained approximately constant during all cycles with a value of $T_{peak_{sol}} \approx 45.4\ ^{\circ}C$. During the solidification process the peak temperature showed a similar behavior. A small hysteresis of 1 °C was observed between the fusion and solidification processes. This value was maintained for all of the samples.

6. Conclusions

The three finer granular PCMs in this work (GR42, 50 and 80) have optimal particle size and density to use in a bubbling fluidized bed. Nevertheless, the materials GR42 and GR80 have agglomeration problems during the fluidization process when the bed temperature is above their transition temperatures. As a consequence, the bed is de-fluidized, and the system behaves similarly to a plug flow system instead of a well-mixed tank. The agglomeration problems have been corroborated by visual inspection in a 2D fluidized bed. After measuring the angle of repose, performing an attrition test and observing the surface of the granular materials with a Scanning Electron Microscope, we conclude that there is no fragmentation of the granular PCMs during the fluidization process, and the cause of the agglomeration problems in GR42 and GR80 is some loss of paraffin because of the particle abrasion during the fluidization process. The paraffin leaks out, stays on the particle surface and acts as a binder. The finer GR50 does not exhibit this problem because it has a thicker boundary structure of SiO_2, which results in a higher mean particle size. The DSC measurements corroborate that the finer GR50 remains stable during 15 cycles of fusion-solidification in a bubbling fluidized bed.

Acknowledgments

Thanks to J. Canales-Vázquez from the Renewable Energy Research Institute of Albacete (Castilla-La Mancha University) for selflessly perform the SEM measurements.

The work is partially funded by the Spanish government (ENE2010-15403, ENE2011-22722 and ENE2015-64117-C5-1). The authors would like to thank the Catalan Government for the quality accreditation to their research groups GREA (2014 SGR 123). The study that led to these results has received funding from the European Union's Seventh Framework Programme (FP7/2007-2013) under grant agreement n° PIRSES-GA-2013-610692 (INNOSTORAGE) and from the European Union's Horizon 2020 research and innovation programme under grant agreement No. 657466 (INPATH-TES).

References

[1] Technology Roadmap. Solar Heating and Cooling. International Energy Agency (IEA); 2012. Available from <www.iea.org> [last accesed December 2015].
[2] Yang J, Yang L, Xu C, Du X. Experimental study on enhancement of thermal energy storage with phase-change material. Appl Energy 2016;169:164–76.
[3] Xu B, Li P, Chan C. Application of phase change materials for thermal energy storage in concentrated solar thermal power plants: a review to recent developments. Appl Energy 2015;160:286–307.
[4] Xia L, Zhang P, Wang RZ. Numerical heat transfer analysis of the packed bed latent heat storage system based on an effective packed bed model. Energy 2010;35:2022–32.
[5] Oró E, Chiu J, Martin V, Cabeza LF. Comparative study of different numerical models of packed bed thermal energy storage systems. Appl Therm Eng 2013;50:384–92.
[6] Rady M. Granular phase change materials for thermal energy storage: experiments and numerical simulations. Appl Therm Eng 2009;29:3149–59.
[7] Izquierdo-Barrientos MA, Sobrino C, Almendros-Ibáñez JA. Thermal energy storage in a fluidized bed of PCM. Chem Eng J 2013;230:573–83.
[8] Peng H, Li R, Ling X, Dong H. Modeling on heat storage performance of compressed air in a packed bed system. Appl Energy 2015;160:1–9.
[9] Pitié F, Zhao CY, Baeyens J, Degrève J, Zhang HL. Circulating fluidized bed heat recovery/storage and its potential to use coated phase-change-material (PCM) particles. Appl Energy 2013;109:505–13.
[10] Izquierdo-Barrientos MA, Sobrino C, Almendros-Ibáñez JA. Energy storage with PCM in fluidized beds: modeling and experiments. Chem Eng J 2015;264:497–505.
[11] Izquierdo-Barrientos MA, Sobrino C, Almendros-Ibáñez JA. Experimental heat transfer coefficients between a surface and fixed and fluidized beds with PCM. Appl Therm Eng 2015;78:373–9.
[12] Izquierdo-Barrientos MA, Sobrino C, Almendros-Ibáñez JA. Modeling the heat transfer coefficient between a surface and fixed and fluidized beds with phase change material. J Heat Transfer: Trans ASME 2016;138:072001.
[13] <www.rubitherm.eu> [last accesed January, 2016].
[14] Geldart D. Types of gas fluidization. Powder Technol 1973;7:285–92.
[15] Sánchez-Delgado S, Almendros-Ibáñez JA, García-Hernando N, Santana D. On the minimum fluidization velocity in 2D fluidized beds. Powder Technol 2011;207:145–53.
[16] Wen CY, Yu YH. A generalized method for predicting the minimum fluidization velocity. AIChE J 1966;12:610–2.
[17] Mahecha-Botero A, Heseidi F, Nguyen A, Li T, Grace JR. Investigation of phase change volumetric flow in fluidized-bed reactors. In: Kim SD, Kang Y, Lee JK, Seo YC, editors. Fluidization XIII: new paradigm in fluidization engineering, engineering conference international. Article 73.
[18] Rees AC, Davidson JF, Dennis JS, Fennell PS, Gladden LF, Hayhurst AN, et al. The nature of the flow just above the perforated plate distributor of a gas-fluidised bed, as imaged using magnetic resonance. Chem Eng Sci 2006;61:6002–15.
[19] Geldart D, Abdullah EC, Hassanpour A, Nwoke LC, Wouters I. Characterization of powder flowability using measurement of angle of repose. China Particuol 2006;4:104–7.
[20] Geldart D, Abdullah EC, Verlinden A. Characterisation of dry powders. Powder Technol 2009;190:70–4.
[21] Krantz K, Zhang H, Zhu J. Characterization of powder flow: static and dynamics testing. Powder Technol 2009;194:239–45.
[22] Antequera MVV, Ruiz AM, Perales MCM, Muñoz NM, Ballesteros MRJC. Evaluation of an adequate method of estimating flowability according to powder characteristics. Int J Pharm 1994;103:155–61.
[23] Werther J, Reppenhagen J. Attrition. In: Yang WC, editor. Handbook of fluidization and fluid-particle systems. New York: Marcel Dekker Inc.; 2013 (Chapter 8).
[24] Ray YC, Jiang TS. Particle attrition phenomena in a fluidized bed. Powder Technol 1987;49:193–206.
[25] Pis JJ, Fuertes AB, Artos A, Suárez A, Rubiera F. Attrition of coal ash particles in a fluidized bed. Powder Technol 1991;66:41–6.
[26] ASTM 2006 Standard test method for determination of attrition and abrasion of powdered catalysts by air jets. Tech. Rep. D5757-00; 2006.
[27] Wu D, Wu F, Gu Z. Catalyst attrition in an ASTM fluidized bed. Catal Today 2016;264:70–4.
[28] Zhao R, Giidwin JG, Jothimurugesan K, Spivey JJ, Gangwal SK. Comparison of attrition test methods: ASTM satandard fluidized bed vs jet cup. Ind Eng Chem Res 2000;39:1155–8.
[29] Lin CL, Peng TH, Wang WJ. Effect of particle size distribution on agglomeration/defluidization during fluidized bed combustion. Powder Technol 2011;207:290–5.
[30] Rady M. Study of phase changing characteristics of granular composites using differential scanning calorimetry. Energy Convers Manage 2009;50:1210–7.
[31] Giro-Paloma J, Barreneche C, Martínez M, Sumiga B, Cabeza LF, Fernández AI. Comparison of phase change slurries: physicochemical and thermal properties. Energy 2015;87:223–7.